

## Emergent non-Hermitian physics in a generalized Lotka-Volterra model

Tengzhou Zhang<sup>1</sup> and Zi Cai<sup>1,2,\*</sup>

<sup>1</sup>*Wilczek Quantum Center and Key Laboratory of Artificial Structures and Quantum Control, School of Physics and Astronomy, Shanghai Jiao Tong University, Shanghai 200240, China*

<sup>2</sup>*Shanghai Research Center for Quantum Sciences, Shanghai 201315, China*



(Received 17 July 2022; revised 5 July 2023; accepted 22 August 2023; published 5 September 2023)

In this paper, we study the non-Hermitian physics emerging from a predator-prey ecological model described by a generalized Lotka-Volterra equation. In the phase space, this nonlinear equation exhibits both chaotic and localized dynamics, which are separated by a critical point. These distinct dynamics originate from the interplay between the periodicity and non-Hermiticity of the effective Hamiltonian in the linearized equation of motion. Moreover, the dynamics at the critical point, such as algebraic divergence, can be understood as an exceptional point in the context of non-Hermitian physics.

DOI: [10.1103/PhysRevB.108.104304](https://doi.org/10.1103/PhysRevB.108.104304)

### I. INTRODUCTION

Physically, non-Hermitian Hamiltonians [1], as a phenomenological description of processes with energy or particles flowing out of the Hilbert space of interest, are responsible for diverse intriguing phenomena in the contexts of classical and quantum waves [2–7], topological physics [8–15], and active matter [16]. Searching for physically transparent examples of non-Hermitian Hamiltonians is not only of fundamental interest for exploring non-Hermitian physics in a broader context, but also of practical significance due to their potential applications in quantum sensing [17,18] and energy transfer [19–21].

In this paper, we propose a generalized Lotka-Volterra equation (GLVE) in a one-dimensional (1D) lattice, which could exhibit chaotic or stable dynamics in different parameter regimes. The Lotka-Volterra (LV) equation describing predator-prey ecological processes is a paradigmatic model in population dynamics [22–24]. Recently, the GLVE has been generalized to spatially periodic systems to study topological phases and edge modes beyond the scope of natural science [25–27]. The dynamics of a slight deviation from the stationary point of the GLVE are governed by a linearized equation resembling the single-particle Schrödinger equation in a lattice system. Therefore topological band theory can straightforwardly be applied to such a classical system [25,26,28]. Here, we show that if the linear expansion is performed around a temporal periodic solution instead of the stationary point of the GLVE, the equation of motion (EOM) of the deviation can also be described by the Schrödinger equation, but with a time-dependent non-Hermitian Hamiltonian. The exponential divergence to chaos and the stable, quasiunitary dynamics both emerge from the Floquet quasienergy band structure. The dynamical critical

point in the original nonlinear model can be understood as an exceptional point of the non-Hermitian Floquet Hamiltonian.

### II. MODEL AND METHOD

#### A. The coupled predator-prey circles

We focus on the GLVE defined in a 1D “diatomic” chain [see Fig. 1(a)], which reads

$$\begin{aligned}\dot{x}_i &= x_i[2 - vy_{i-1} - wy_i], \\ \dot{y}_i &= y_i[-2 + vx_i + wx_{i+1}],\end{aligned}\quad (1)$$

where  $i = 1 \cdots L$ , with  $L$  being the number of unit cells, each of which contains a prey ( $x_i$ ) and a predator ( $y_i$ ).  $v = 1 + r$  and  $w = 1 - r$ ;  $0 < r < 1$  is the only tunable parameter in Eq. (1) characterizing the difference between the inter- and intra-unit-cell coupling strengths. The linear terms on the right-hand side of Eq. (1) suggest an exponential growth (decay) for the prey (predator) populations if there is no interspecies interaction, while the nonlinear terms indicate the interaction between one species and its neighbors, which suppresses the exponential growth (decay).

Starting with a simple situation where the populations of prey and predators are site independent  $x_i(t) = x(t)$ ,  $y_i(t) = y(t)$ , Eq. (1) is reduced to a two-species LV equation:

$$\begin{aligned}\dot{x} &= 2x - 2xy, \\ \dot{y} &= -2y + 2xy,\end{aligned}\quad (2)$$

which is commonly used to explain the oscillation behavior of natural populations (e.g., the snowshoe hare and lynx) in ecological systems with predator-prey interactions, competition, and disease. Mathematically, this model is integrable with a constant of motion [24],  $V = x + y - \ln xy - 2$ . Consequently, it supports either a steady solution  $[x^*, y^*]^T = [1, 1]^T$  (with  $V = 0$ ) or a periodic oscillation  $[\bar{x}(t), \bar{y}(t)]^T$  (with  $V > 0$ ) [see Fig. 1(b)], corresponding to a fixed point or a closed orbit around the fixed point in the phase space, respectively [see Fig. 1(c)].

\*zcai@sjtu.edu.cn

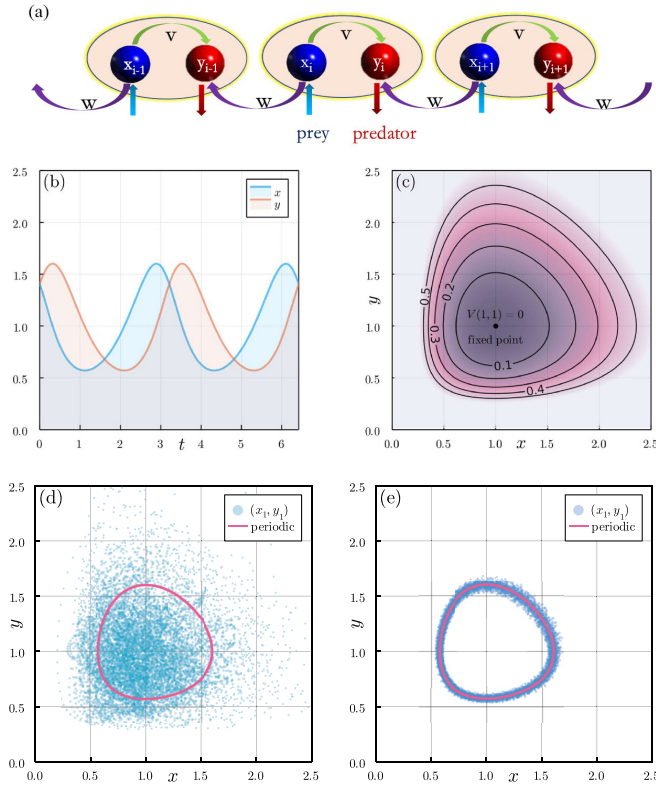


FIG. 1. (a) Predator-prey model defined in a 1D “diatomic” chain described by the GLVE (1). (b) Periodic solution  $[\bar{x}(t), \bar{y}(t)]^T$  of the homogeneous GLVE (2) with the conserved quantity  $V = 0.131$ . (c) Trajectories of  $[\bar{x}(t), \bar{y}(t)]^T$  in the phase space with different conserved quantities. (d) and (e) Trajectories in the phase space of the first unit cell ( $i = 1$ ) predicted via the GLVE (1) with  $\Delta = 0.05$ ,  $L = 1024$ , and either  $r = 0.3$  (d) or  $r = 0.7$  (e). The initial state of (d) and (e) is spatially inhomogeneous:  $\delta_i(t = 0) = \Delta_i$ , with  $\Delta_i$  being randomly sampled from  $[-\Delta, \Delta]$ . The red curves indicate the trajectory starting from the spatially homogeneous initial state  $\delta_i(t = 0) = 0$ .

In general, one needs to take the spatial fluctuation into account. Considering a solution  $v(t) = [x_1, y_1, \dots, x_L, y_L]^T$  of Eq. (1), one can expand it around the spatially homogeneous solutions as

$$v_i(t) = [1 + \delta_i(t)]\bar{v}_i(t), \quad (3)$$

where  $\delta(t) = [\delta_1^x(t), \delta_1^y(t), \dots]^T$  [ $\delta_i^x(t) = \frac{x_i(t) - \bar{x}(t)}{\bar{x}(t)}$ , and  $\delta_i^y(t)$  is likewise].  $\bar{v}$  donates an unperturbed solution and is not necessarily spatially homogeneous. A linearized equation can be derived in terms of the dimensionless vector  $\delta(t)$ .

### B. Linear expansion around the stationary solution

For a homogeneous stationary solution  $\bar{v}^*(t) = [1, 1, \dots, 1, 1]^T$ , it is shown that the linearized EOM of  $\delta(t)$  takes the identical form of the single-particle Schrödinger equation in a 1D lattice:

$$i \frac{d\delta(t)}{dt} = H\delta(t), \quad (4)$$

where  $H = H_0$  is a time-independent  $2L \times 2L$  antisymmetric Hermitian matrix (due to the prefactor  $i$ )

$$H_0 = i \begin{bmatrix} 0 & -v & & -w \\ v & 0 & w & \\ & -w & 0 & -v \\ & & v & 0 & \ddots \\ & & & \ddots & \ddots \\ w & & & & & \ddots \end{bmatrix}. \quad (5)$$

### C. Linear expansion around the periodic solution

Unlike previous studies [25,26], here we expand the nonlinear equation (1) around the periodic solution  $\bar{v}_p(t) = [\bar{x}(t), \bar{y}(t), \dots, \bar{x}(t), \bar{y}(t)]^T$ , where  $\bar{x}(t), \bar{y}(t)$  are the solution of Eq. (2) with a period  $T \approx \pi$ . The linearized EOM takes the same form as Eq. (4), but with a time-dependent non-Hermitian “Hamiltonian”

$$H(t) = H_0 D(t), \quad (6)$$

where  $H_0$  has the same definition as Eq. (5) and  $D(t)$  is a diagonal matrix with dimension  $2L$ :

$$D(t) = \begin{bmatrix} \bar{x}(t) & & & & \\ & \bar{y}(t) & & & \\ & & \ddots & & \\ & & & \bar{x}(t) & \\ & & & & \bar{y}(t) \end{bmatrix}. \quad (7)$$

## III. CHAOTIC VERSUS LOCALIZED DYNAMICS IN THE PHASE SPACE

Before discussing the linearized EOM, we first focus on the dynamics of the nonlinear equation (1), which can be solved using the standard Runge-Kutta method. A key question is whether the spatially homogeneous periodic solution  $[\bar{x}(t), \bar{y}(t)]^T$  is stable against spatial fluctuations. To address this issue, we impose a small site-dependent perturbation on the initial state as  $\delta_i(t = 0) = \Delta_i$ , where  $\Delta_i$  is randomly sampled from a uniform random distribution with  $\Delta_i \in [-\Delta, \Delta]$  and  $\Delta \ll 1$  [for a spatially homogeneous solution,  $\delta_i(t = 0) = 0$ ]. We first study the dynamics in one unit cell (say,  $i = 1$ ) by plotting the trajectories of  $x_1(t)$  and  $y_1(t)$  in the phase space. As shown in Fig. 1(d), for a small  $r$  (e.g.,  $r = 0.3$ ), the trajectory of  $[x_1(t), y_1(t)]^T$  rapidly deviates from the spatially homogeneous solution  $[\bar{x}(t), \bar{y}(t)]^T$  after a short time, while randomly walking in the phase space on long timescales, indicating that the solution  $[\bar{x}(t), \bar{y}(t)]^T$  is unstable against spatial fluctuation for small  $r$ . Conversely, at a relatively large  $r$  (e.g.,  $r = 0.7$ ), the trajectory of  $[x_1(t), y_1(t)]$  is bounded within a finite regime around  $[\bar{x}(t), \bar{y}(t)]$  [see Fig. 1(e)].

The qualitatively different dynamical behaviors between the cases with small and large values of  $r$  reveal a nonequilibrium phase transition, which can be characterized by the average deviation:  $\sigma(t) = \sqrt{\frac{1}{L} \sum_i [\delta_i^x(t)]^2 + [\delta_i^y(t)]^2}$ . As shown in Fig. 2,  $\sigma(t)$  increases exponentially (accompanied by an oscillation) at small  $r$  (a signature of chaos), while it keeps oscillating around a finite value at large  $r$ . The exponent of the exponential divergence approaches zero at critical  $r = r_c$ , whose value depends on the amplitude of the periodic oscillation of the spatially homogeneous solutions.

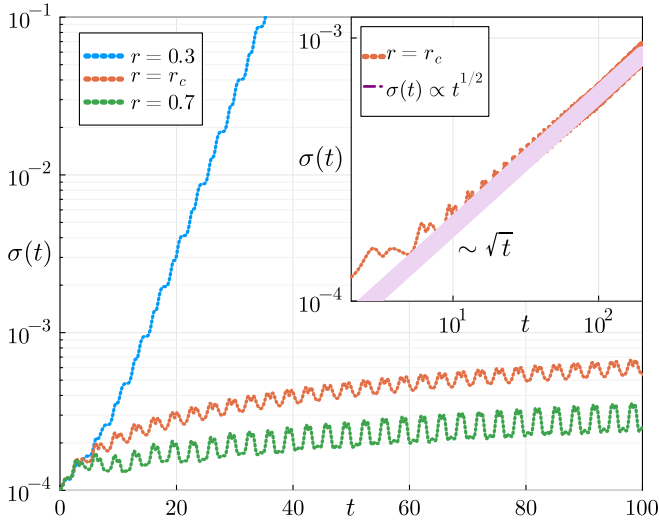


FIG. 2. Dynamics of the average deviation  $\sigma(t)$  with different  $r$  values in a semilog plot ( $r_c = 0.64579$  is the critical point). The inset presents the dynamics of  $\sigma(t)$  at the critical point in the log-log plot. The initial state is chosen as  $x_i(t=0) = y_i(t=0) = 1.6(1 + \Delta_i)$ , where the amplitude of the periodic solution  $\xi \approx 0.33$  and  $\Delta_i$  is randomly sampled from  $[-\Delta, \Delta]$ , where  $\Delta = 2 \times 10^{-4}$ .

At the dynamical critical point,  $\sigma(t)$  grows algebraically as  $\sigma(t) \sim t^{1/2}$ . In the following, we will explain these observed dynamical behaviors as well as the critical dynamics based on the properties of the non-Hermitian Hamiltonian in Eq. (6).

#### IV. FLOQUET DYNAMICS WITH A NON-HERMITIAN HAMILTONIAN

Now we focus on the linearized EOM (4), where the time-dependent Hamiltonian (6) is non-Hermitian but periodic in time  $H(t) = H(t + T)$ . However, unlike the intensively studied cases with a periodically driven Hamiltonian, the periodic oscillation in Hamiltonian equation (6) is not due to external driving; rather, it originates from the spontaneous oscillation in the time-independent GLVE (1) and is self-sustained. Thanks to the spatially translational invariance, one can perform the Fourier transformation, after which the EOM (4) turns into a collection of independent  $k$  modes, each of which is a two-level system governed by the EOM

$$i \frac{d\delta_k}{dt} = H_k(t)\delta_k, \quad (8)$$

where  $\delta_k = [\delta_k^x, \delta_k^y]^T$  with  $\delta_k^x = \frac{1}{\sqrt{L}} \sum_j e^{-ikj} \delta_j^x$  and  $\delta_k^y$  being likewise.  $H_k$  is a  $2 \times 2$  matrix defined as

$$H_k(t) = H_k^0 D(t), \quad (9)$$

with

$$H_k^0 = \begin{bmatrix} 0 & -i(v + we^{-ik}) \\ i(v + we^{ik}) & 0 \end{bmatrix}, \quad (10)$$

$$D(t) = \begin{bmatrix} \bar{x}(t) & \\ & \bar{y}(t) \end{bmatrix}.$$

Again,  $H_k$  is non-Hermitian if  $\bar{x}(t) \neq \bar{y}(t)$ . Its instantaneous eigenvalues are still real, but the dynamics is not trivial, since

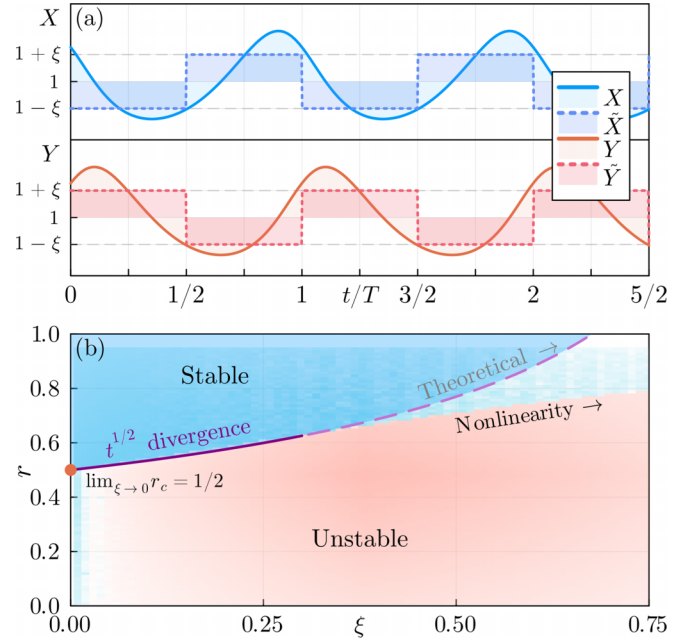


FIG. 3. (a) Sketch of the step-function approximation where the periodic solutions  $[\bar{x}(t), \bar{y}(t)]^T$  are replaced by the step functions  $[\tilde{x}(t), \tilde{y}(t)]^T$ . (b) The phase diagram obtained with the simplified model (separated by the dashed line) and the numerical result of the phase diagram (heat map in the background). The heat map displays  $\sigma(t)$  after a long time ( $t = 600$ ), which remains as small as  $\Delta$  (blue) for the stable phase and saturates to a large value of roughly 1 for the divergent phase (red).

generally  $[H_k(t_1), H_k(t_2)] \neq 0$ . Both  $\bar{x}(t)$  and  $\bar{y}(t)$  are periodic in time with a period  $T$ , enabling us to employ the Floquet description of the dynamics of Eq. (8) and derive a time-independent Floquet Hamiltonian  $H_k^F$  satisfying

$$\mathcal{F}_k = e^{-iH_k^F T} = \mathcal{T} e^{-i \int_0^T dt H_k(t)}, \quad (11)$$

where  $\mathcal{T}$  is the time-ordering operator and  $\mathcal{F}_k$  is the evolution operator for the  $k$  mode within one period which is not necessarily unitary [29].

##### A. Step-function approximation

The periodic solution  $[\bar{x}(t), \bar{y}(t)]^T$  does not have a closed-form expression; thus it is impossible to analytically perform the time-ordering integral in Eq. (11) and derive an explicit form of the Floquet operator, even for a  $2 \times 2$  matrix. As we will show in the following, the qualitative dynamical behavior and the critical properties of our model do not crucially depend on the explicit formalism of the periodic function; what really matters is the amplitude and the period of the periodic function. Therefore, to analytically understand the different dynamical behaviors and the transition between them, we adopt an approximation by replacing the diagonal matrix in Eq. (10) with a simplified formalism as [see Fig. 3(a)]

$$D(t) = \begin{cases} \mathbb{I} + \xi \delta^z, & nT < t < (n + \frac{1}{2})T \\ \mathbb{I} - \xi \delta^z, & (n + \frac{1}{2})T < t < (n + 1)T, \end{cases} \quad (12)$$

where  $n$  is an integer,  $\mathbb{I}$  represents a  $2 \times 2$  identity matrix, and  $\hat{\sigma}^z$  denotes the  $z$ -component Pauli matrix. Furthermore,  $\xi \in [0, 1]$  characterizes the amplitude of the periodic oscillation, which is determined by the initial conditions in the original LV equation obtained by requiring that the step function share the same first-order Fourier coefficient with the periodic solution  $\bar{x}(t)$ ,  $\bar{y}(t)$ :

$$\int_0^T dt e^{-i\omega t} \cdot 2\xi \operatorname{sgn}(\sin \omega t) = \int_0^T dt e^{-i\omega t} [\bar{x}(t) - \bar{y}(t)]. \quad (13)$$

If the nonlinearity is small, so that harmonic approximation can be applied to  $\bar{x}(t)$ ,  $\bar{y}(t)$ ,  $\xi$  is simply promotional to the homogeneous oscillation amplitude:

$$\xi = \frac{\pi}{8} \sqrt{[(\bar{x}(t) - x^*)^2 + (\bar{y}(t) - y^*)^2]}. \quad (14)$$

### B. Quasienergy band and the phase diagram of dynamical stability

In the following, we demonstrate that despite the simplicity of such a step-function approximation, it can capture the essence of the non-Hermitian Floquet physics as well as the critical behavior and explain the two different dynamics observed in the nonlinear equation (1). By introducing  $H_k^\pm = H_k^0(\mathbb{I} \pm \xi \sigma_z)$ , the evolution operator becomes

$$\mathcal{F}_k = e^{-i\frac{T}{2}H_k^+} e^{-i\frac{T}{2}H_k^-} = \begin{bmatrix} \frac{\cos \phi_k + \xi}{1 + \xi} & -\frac{ie^{i\phi_k} \sin \phi_k}{\sqrt{1 - \xi^2}} \\ -\frac{ie^{-i\phi_k} \sin \phi_k}{\sqrt{1 - \xi^2}} & \frac{\cos \phi_k - \xi}{1 - \xi} \end{bmatrix}, \quad (15)$$

where  $\phi_k = \frac{\Delta_k T}{2} \sqrt{1 - \xi^2}$  and  $\Delta_k$  is the energy gap of  $H_k^0$  [ $\Delta_k = 2\sqrt{(2 + 2\cos k) + 2(1 - \cos k)r^2}$ ].  $\phi_k = \arg[-i(v + we^{-ik})]$ . By diagonalizing the matrix presented in Eq. (15), one can obtain the eigenvalues of  $\mathcal{F}_k$ :

$$\lambda_k = \frac{\cos \phi_k - \xi^2 \pm 2i \left| \sin \frac{\phi_k}{2} \right| \sqrt{\cos^2 \frac{\phi_k}{2} - \xi^2}}{1 - \xi^2}. \quad (16)$$

Notably, the properties of  $\lambda_k$  considerably depend on the sign of  $\cos^2 \frac{\phi_k}{2} - \xi^2$ , resulting in qualitatively different physical consequences. If  $\cos^2 \frac{\phi_k}{2} > \xi^2$  for all the  $k$  modes, it is easy to check that  $|\lambda_k| = 1$ ; therefore we can introduce a real number  $\theta_k \in [0, 2\pi]$  such that  $\lambda_k = e^{\pm i\theta_k}$ . Let  $\varepsilon_k$  be the quasienergy of the Floquet Hamiltonian  $H_k^F$ ; since  $H_k^F = \frac{i}{T} \ln \mathcal{F}_k$ , one can obtain  $\varepsilon_k = \frac{i}{T} \ln \lambda_k = \mp \frac{\theta_k}{T}$ . Therefore, in this case all the eigenvalues of the Floquet Hamiltonian  $H_k^F$  are real, and the dynamics of evolution remains stable. Consequently, there is no divergence for the deviation, and the dynamics is bounded within a finite regime around the homogeneous trajectory  $[\bar{x}(t), \bar{y}(t)]$ , agreeing with our numerical observation for large  $r$ . In contrast, when  $\cos^2 \frac{\phi_k}{2} < \xi^2$ ,  $\lambda_k$  defined in Eq. (16) becomes real, and  $|\lambda_k| \neq 1$ . As a consequence, the eigenvalue of the Floquet Hamiltonian  $\varepsilon_k$  is no longer real, but with a pair of opposite imaginary parts, among which the positive imaginary part is responsible for the exponential divergence of the deviation observed in the case with small  $r$ . Obviously, such an exponential divergence predicted by the linear analysis cannot persist forever, because

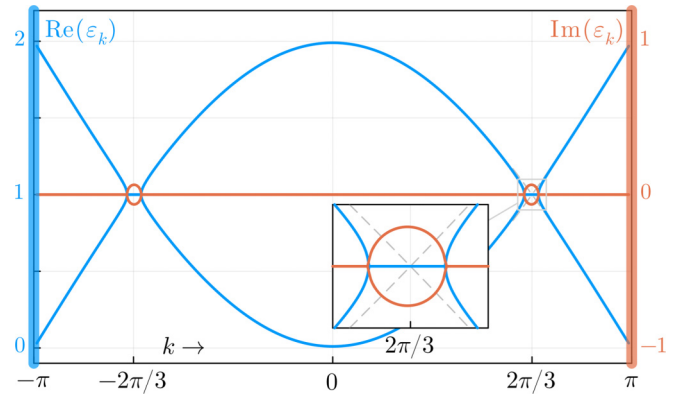


FIG. 4. Floquet quasienergy band structure of a typical unstable case, where  $\xi = 0.1$ ,  $r = 0$ . The inset magnifies the region where the real parts of the quasienergy become degenerate and the imaginary parts split into conjugate pairs.

the nonlinear effect will finally take over and governs the long-time dynamics.

To illustratively address this mechanism, we numerically calculate one quasienergy band in the unstable phase; see Fig. 4. The imaginary parts of  $\varepsilon_k$  are nonzero near  $\Delta_k(k^*) = \omega$ , which is just  $k^* \approx 2\pi/3$ . Any initial noise near  $k^*$  gets amplified and exponentially grows. In contrast, at relatively large  $r$ , if there is no such splitting of imaginary parts in the band, the dynamics stays quasiunitary and stable.

It would also be interesting to analytically investigate the Lyapunov exponent of the divergence, named  $\eta$ , which corresponds to the maximum of the imaginary part of the quasienergy. Near  $k^* = \operatorname{argmax}[\operatorname{Im} \varepsilon_k(k)]$ , we introduce the detuning parameter  $v = \frac{\omega}{\Delta_k^*} - 1$  and neglect  $O(\xi^2)$  and smaller terms so that one can approximately obtain

$$\varepsilon_k = \begin{cases} 1 \pm \sqrt{v^2 - v_c^2}, & |v| > v_c \\ 1 \pm i\sqrt{v_c^2 - v}, & |v| \leq v_c, \end{cases} \quad (17)$$

where  $v_c = 2\xi/\pi$  is proportional to  $\xi$ . To this first-order approximation,  $\eta = v_c = 2\xi/\pi$  and does not depend on  $r$  (there is a tiny dependence on  $r$  considering high-order terms, and this approximation fails when  $|r - r_c|$  is comparable to  $\xi$  or the system is totally stable). This approximation agrees well with the accurate calculation shown in the inset of Fig. 4.

Besides quantitatively explaining the Lyapunov component of divergence, we can further determine the critical condition for the system to be stable: The energy gap of  $H_k^0$  satisfies  $\Delta_k \in [4r, 4]$  ( $0 < r < 1$ ), which takes its minimum value  $\Delta_{\min} = 4r$  at  $k = \pi$ . Therefore, for  $\xi$  fixed by small oscillation amplitude, the  $\pi$  mode ( $k = \pi$ ) will first become unstable as  $r$  decreases below the critical value  $r_c$  that satisfies  $\cos[\pi r_c \sqrt{1 - \xi^2}] = -\xi$ , which indicates that  $r_c \rightarrow \frac{1}{2}$  in the limit of  $\xi \rightarrow 0$ .

The phase diagram under this step-function approximation is also determined and plotted using the smooth line in Fig. 3(b), where the phase boundary  $r_c(\xi)$  is determined by the condition  $\cos[\pi r_c \sqrt{1 - \xi^2}] = -\xi$ , at which the  $\pi$  mode starts to be unstable. The overlapped heat map is the phase diagram from numerical simulation of the nonlinear GLVE (1) and agrees with the approximation. Both results show that  $r_c \rightarrow \frac{1}{2}$

when  $\xi \rightarrow 0$ , indicating that the approximation becomes exact in the limit of  $\xi \rightarrow 0$  (but is still illustrative for any small  $\xi$ ). For relatively large  $\xi$ , the nonlinearity cannot be neglected and leads to a shift of the boundary between the two phases.

## V. CRITICAL DYNAMICS: AN EMERGENT EXCEPTIONAL POINT

In this section, we will explain the  $t^{\frac{1}{2}}$  divergence of the average deviation  $\sigma(t)$  observed right at the critical point, which can be understood as a collective behavior of the  $k$  modes close to  $k = \pi$ .

$$\sigma^2(t) = \frac{1}{L} \sum_i \delta_i(t) \delta_i(t) = \frac{1}{L} \sum_k \delta_k(t) \delta_{-k}(t), \quad (18)$$

where the momentum summation is over the  $k$  mode in the first Brillouin zone  $k \in [0, 2\pi]$  and  $\delta_k(t) = [\delta_k^x(t), \delta_k^y(t)]^T$ .

### A. Dynamics of modes right at the exceptional point

Right at the critical point, we first focus on the  $\pi$  mode, whose dynamics at integer multiples of the period  $T$  ( $t = nT$ ) is governed by the Floquet operator

$$\mathcal{F}_\pi = 2\xi \begin{bmatrix} 1 & -1 \\ 1 & -1 \end{bmatrix} + \begin{bmatrix} -1 & 0 \\ 0 & -1 \end{bmatrix}. \quad (19)$$

Such a  $2 \times 2$  matrix has parallel eigenvectors with a degenerate eigenvalue  $\lambda_\pi = -1$ , indicating that it is an exceptional point for the non-Hermitian matrix  $\mathcal{F}_\pi$ . Next, we will study the long-time dynamics governed by  $\mathcal{F}_\pi$ .

The dynamics of  $\delta_\pi(t)$  with  $t = nT$  can be directly expressed as

$$\delta_\pi(nT) = \mathcal{F}_\pi^n \delta_\pi(0). \quad (20)$$

Assuming that initially  $\delta_\pi(0) = [a, b]^T$ , from Eq. (20), one can derive that

$$\delta_\pi(t) = (-1)^n \left\{ a \begin{bmatrix} 1 - Kt \\ -Kt \end{bmatrix} + b \begin{bmatrix} Kt \\ 1 + Kt \end{bmatrix} \right\}, \quad (21)$$

where  $t = nT$ ,  $K = \frac{2\xi}{T}$ . In the long-time limit  $t \gg 1/K$ , Eq. (21) is reduced to

$$\delta_\pi(t) = (b - a)Kt \begin{bmatrix} 1 \\ 1 \end{bmatrix}, \quad (22)$$

which indicates a linear divergence of  $|\delta_\pi(t)|$  at the critical point. This agrees very well with the numerical results as shown in Fig. 5, where the envelope of  $|\delta_\pi(t)|$  grows linearly in time.

### B. Collective behavior of modes and algebraic divergence

For a single mode, the dynamics is either staying stable or diverging linearly, which indicates that the  $1/2$  power-law sublinear divergence is a collective behavior under the thermodynamic limit. According to Eq. (18), all the  $k$  modes contribute to  $\sigma(t)$ , while at the critical point, only the  $\pi$  mode and those  $k$  modes close to it dominate the long-time dynamics of  $\sigma(t)$ . Now we focus on those  $k$  modes close to the  $\pi$  mode with  $k = \pi + q$  and  $q \ll 1$ . As shown in Fig. 5, for a  $k$  mode that slight deviates from  $k = \pi$ , the envelope

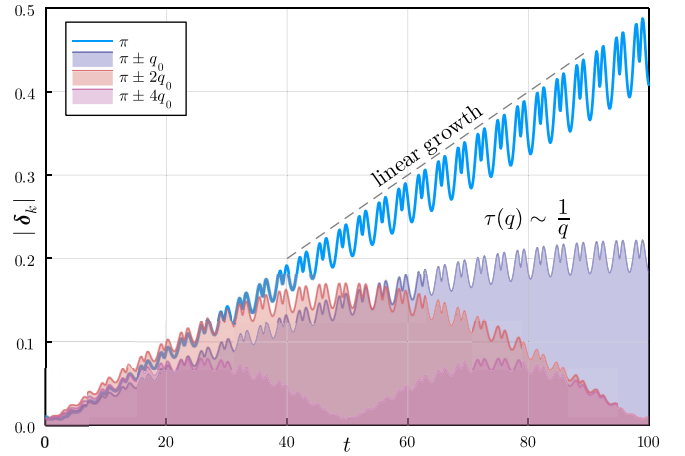


FIG. 5. The dynamics of  $|\delta_k|$  for different  $k$  modes that are right at or close to  $k = \pi$ .  $q_0 = \frac{\pi}{64}$ .

of  $|\delta_{\pi+q}(t)|$  behavior resembles a sine function: Initially, it grows linearly in time, while after a characteristic timescale  $t_q^*$ , it will significantly deviate from the linear function. Such a characteristic timescale is roughly a quarter of the period of the sine function, which in turn, is proportional to  $1/|q|$ , as shown in Fig. 5.

We can phenomenologically describe the dynamics of  $\delta_{\pi+q}$  with

$$|\delta_{\pi+q}(t)| = A_q \left| \frac{q_0}{q} \sin \left( \frac{q}{q_0} Kt \right) \right|, \quad (23)$$

where  $A_q$  is a random amplitude but of the same order for all  $q$ .  $q_0$  is a characteristic constant for all  $q$ . In this approximation,  $t_q^* \sim Kq_0/|q| \sim |q|^{-1}$ . Also, the linear growth of the  $\pi$  mode is recovered in the limit that  $q \rightarrow 0$ .

Qualitatively, the closer a  $k$  mode is to  $k = \pi$ , the longer it can contribute a linear component to  $\sigma(t)$ . At a fixed time  $t$ , only  $\mathcal{N}(t) \sim 1/t$  of those  $k$  modes satisfy  $t_q^* > t$  and are still linearly growing, which explains why the collective dynamics of  $\sigma(t)$  is sublinear. Quantitatively, by substituting the phenomenological expression for  $\delta_{\pi+q}(t)$  of Eq. (23), we can explicitly calculate  $\sigma(t)$ :

$$\begin{aligned} \sigma^2(t) &= \int_{-\pi}^{+\pi} dq \rho(q) |\delta_{\pi+q}(t)|^2 \\ &\approx \langle A_q^2 \rangle \frac{N}{2\pi} Kt q_0 \int_{-\infty}^{+\infty} dx \frac{\sin^2 x}{x^2} = \frac{NKq_0}{2} \langle A_q^2 \rangle \cdot t, \end{aligned} \quad (24)$$

where the amplitude  $A_q$  is assumed to be uniform over all  $q$  and replaced by its average  $\langle A_q \rangle$  over  $q$ . Therefore one can obtain  $\sigma(t) \sim t^{1/2}$ , which agrees with the critical power-law divergence of the nonlinear GLVE.

## VI. CONCLUSION AND OUTLOOK

In summary, this study shows that non-Hermitian physics, which used to be considered as a consequence of dissipative quantum systems, can emerge in classical nonlinear systems out of equilibrium. This work also provides an alternative

member to the quasi-Hermitian family with real eigenvalues. It is shown that the interplay between temporal periodicity and non-Hermiticity can lead to intriguing dynamic behaviors [29–36].

We also point out that the expansion technique in Eq. (3) can be applied to other predator-prey-type GLVEs, which results in a Hamiltonian like Eq. (9) that is usually time dependent and non-Hermitian; see the Appendix. Our method also provides an opportunity to understand phenomena such as pattern formation [37] and phase coexistence [38] in GLVEs from the perspective of non-Hermitian physics.

### ACKNOWLEDGMENTS

This work is supported by the National Key Research and Development Program of China (Grant No. 2020YFA0309000), NSFC of China (Grant No. 12174251), Natural Science Foundation of Shanghai (Grant No. 22ZR142830), and Shanghai Municipal Science and Technology Major Project (Grant No. 2019SHZDZX01). Z.C. thanks the Yangyang Development Fund for its sponsorship.

### APPENDIX: DERIVATION OF TIME-DEPENDENT NON-HERMITIAN HAMILTONIANS FROM GENERIC GLVEs

Mathematically, GLVEs can be written in the generic form where all variables and parameters are real valued:

$$\dot{x}_i = x_i \left( \gamma_i + \sum_{j \neq i} \kappa_{ij} x_j \right), \quad (\text{A1})$$

where  $x_i$  denotes the mass on site  $i$  and is usually considered positive.  $\gamma_i$  is the corresponding growth or decay rate. The coupling coefficients  $\kappa_{ij}$  characterize the nonlinear interaction among sites.

Now we focus on the evolution of perturbation  $\delta_i(t)$  on a given solution  $X_i(t)$  (not necessarily periodic or stationary). Substituting  $x_i(t) = [1 + \delta_i(t)]X_i(t)$ , we get

$$(1 + \delta_i)\dot{X}_i + X_i\dot{\delta}_i = (1 + \delta_i)X_i \left[ \gamma_i + \sum_{i \neq j} \kappa_{ij} X_j (1 + \delta_j) \right], \quad (\text{A2})$$

and by neglecting  $o(\delta^2)$  terms such as  $\delta_i\delta_j$ , we obtain an EOM for  $\delta_i$  that does not explicitly contain  $\gamma_i$ :

$$\dot{\delta}_i = \kappa_{ij} X_j \delta_j. \quad (\text{A3})$$

Now let us use the following more heuristic symbols:

$$D_{ij}(t) = X_i(t)\delta_{i,j}, \quad \{H_0\}_{ij} = i\kappa_{ij}, \quad (\text{A4})$$

where  $D = \text{diag}[X_1(t) \cdots X_n(t)]$  is a diagonal matrix. Now we multiply EOM (A3) by a factor of  $i$ . Then it turns out to be

$$i \frac{d\delta_i}{dt} = \{H_0\}_{ij} D_{jk} \delta_k, \quad (\text{A5})$$

or

$$i \frac{d}{dt} \delta = H_0 D(t) \delta, \quad (\text{A6})$$

which is essentially a single-particle Schrödinger equation with a time-dependent non-Hermitian ‘‘Hamiltonian’’

$$H(t) = H_0 D(t). \quad (\text{A7})$$

For predator-prey models,  $\kappa_{ij}$  are sign constrained such that  $\kappa_{ij}\kappa_{ji} < 0$  and are called antagonistic [39], where the anti-symmetric ( $\kappa_{ij} = -\kappa_{ji}$ ) case is often of interest [25,28,38]. If the latter is true, then  $H_0^\dagger = H_0$ , and  $H_0$  will be Hermitian. Moreover, the generic GLVE (A1) can be written as

$$\dot{y}_i = \gamma_i + \sum_{j \neq i} \kappa_{ij} \exp y_j, \quad (\text{A8})$$

where  $y_i = \log x_i$ , where we can infer that  $\forall X_i(t)$  will stay positive as long as  $\forall X_i(t=0) > 0$ . Therefore  $D(t)$  is positive semidefinite, and Cholesky factorization  $L^\dagger L = D$  is well defined with  $L = \sqrt{D}$ . It is easy to check that  $H = H_0 D$  is similar to another Hermitian Hamiltonian  $\mathcal{H} = L^\dagger H_0 L$ :

$$H = (L^\dagger)^{-1} \mathcal{H} L^\dagger. \quad (\text{A9})$$

This guarantees that  $H$  share the same eigenvalues  $\{\omega_i\}$  with  $\mathcal{H}$ , which are real; their eigenvectors  $\{\psi_i\}$  for  $H$  and  $\{\phi_i\}$  for  $\mathcal{H}$  are usually different but can be related by the transformation

$$\phi_i = L^\dagger \psi_i = \sqrt{D} \psi_i. \quad (\text{A10})$$

Since  $\det \sqrt{D} = \sqrt{\prod_{i=1}^N X_i(t)} > 0$ , the inverse transformation

$$\psi_i = (L^\dagger)^{-1} \phi_i = D^{-\frac{1}{2}} \phi_i \quad (\text{A11})$$

is well defined and keeps the span  $\{\psi_i\}$  nondegenerate.

If one performs such an expansion around a saturated solution  $X_j(t) = X_j^*$ , then  $H$  is time independent. Despite the non-Hermiticity of  $H$ , this will not lead to more intriguing dynamics than  $H'$ . One would expect quasiunitary dynamics and will not encounter exceptional points because the non-degeneracy of  $\{\psi_i\}$  means that none of the eigenvectors is parallel to another.

In contrast, nontrivial dynamics lies behind the time dependence of  $H(t)$ . If  $[H(t_1), H(t_2)] \neq 0$ , then the effective Hamiltonian on a given time interval can possibly be  $\mathcal{PT}$ -broken with complex eigenvalues or host exceptional points with parallel eigenvectors, exhibiting nontrivial dynamics. Additionally, Floquet analysis can be applied if the solution  $X_i(t)$  is periodic.

[1] Y. Ashida, Z. Gong, and M. Ueda, *Adv. Phys.* **69**, 249 (2020).

[2] A. Ruschhaupt, F. Delgado, and J. G. Muga, *J. Phys. A: Math. Gen.* **38**, L171 (2005).

[3] C. E. Ruter, K. G. Makris, R. El-Ganainy, D. N. Christodoulides, M. Segev, and D. Kip, *Nat. Phys.* **6**, 192 (2010).

- [4] B. Peng, S. K. Ozdemir, F. Lei, F. Monifi, M. Gianfreda, G. L. Long, S. H. Fan, F. Nori, C. M. Bender, and L. Yang, *Nat. Phys.* **10**, 394 (2014).
- [5] L. Feng, Z. J. Wong, R. M. Ma, Y. Wang, and X. Zhang, *Science* **346**, 972 (2014).
- [6] K. Bertoldi, V. Vitelli, J. Christensen, and M. van Hecke, *Nat. Rev. Mater.* **2**, 17066 (2017).
- [7] L. Xiao, T. Deng, K. Wang, G. Zhu, Z. Wang, W. Yi, and P. Xue, *Nat. Phys.* **16**, 761 (2020).
- [8] T. E. Lee, *Phys. Rev. Lett.* **116**, 133903 (2016).
- [9] S. Yao and Z. Wang, *Phys. Rev. Lett.* **121**, 086803 (2018).
- [10] S. Yao, F. Song, and Z. Wang, *Phys. Rev. Lett.* **121**, 136802 (2018).
- [11] Z. Gong, Y. Ashida, K. Kawabata, K. Takasan, S. Higashikawa, and M. Ueda, *Phys. Rev. X* **8**, 031079 (2018).
- [12] C.-H. Liu, H. Jiang, and S. Chen, *Phys. Rev. B* **99**, 125103 (2019).
- [13] D. S. Borgnia, A. J. Kruchkov, and R.-J. Slager, *Phys. Rev. Lett.* **124**, 056802 (2020).
- [14] E. J. Bergholtz, J. C. Budich, and F. K. Kunst, *Rev. Mod. Phys.* **93**, 015005 (2021).
- [15] X.-R. Wang, C.-X. Guo, and S.-P. Kou, *Phys. Rev. B* **101**, 121116(R) (2020).
- [16] M. Fruchart, R. Hanai, P. B. Littlewood, and V. Vitelli, *Nature (London)* **592**, 363 (2021).
- [17] W. Chen, S. K. Ozdemir, G. Zhao, J. Wiersig, and L. Yang, *Nature (London)* **548**, 192 (2017).
- [18] H. Hodaei, A. U. Hassan, S. Wittek, H. Garcia-Gracia, R. El-Ganainy, D. N. Christodoulides, and M. Khajavikhan, *Nature (London)* **548**, 187 (2017).
- [19] S. Assaworarith, X. Yu, and S. Fan, *Nature (London)* **546**, 387 (2017).
- [20] H. Xu, D. Mason, L. Jiang, and J. G. E. Harris, *Nature (London)* **537**, 80 (2016).
- [21] J. C. Budich and E. J. Bergholtz, *Phys. Rev. Lett.* **125**, 180403 (2020).
- [22] A. J. Lotka, *J. Phys. Chem.* **14**, 271 (1910).
- [23] J. Volterra, *ICES J. Mar. Sci.* **3**, 3 (1928).
- [24] N. S. Goel, S. C. Maitra, and E. W. Montroll, *Rev. Mod. Phys.* **43**, 231 (1971).
- [25] J. Knebel, P. M. Geiger, and E. Frey, *Phys. Rev. Lett.* **125**, 258301 (2020).
- [26] T. Yoshida, T. Mizoguchi, and Y. Hatsugai, *Phys. Rev. E* **104**, 025003 (2021).
- [27] E. Tang, J. Agudo-Canalejo, and R. Golestanian, *Phys. Rev. X* **11**, 031015 (2021).
- [28] M. Umer and J. Gong, *Phys. Rev. B* **106**, L241403 (2022).
- [29] H. Wu and J.-H. An, *Phys. Rev. B* **102**, 041119(R) (2020).
- [30] J. Li, A. K. Harter, J. Liu, L. de Melo, Y. N. Joglekar, and L. Luo, *Nat. Commun.* **10**, 855 (2019).
- [31] S. Longhi, *J. Phys. A: Math. Theor.* **50**, 505201 (2017).
- [32] T. T. Koutserimpas and R. Fleury, *Phys. Rev. Lett.* **120**, 087401 (2018).
- [33] L. Zhou and J. Gong, *Phys. Rev. B* **98**, 205417 (2018).
- [34] L. Zhou, *Phys. Rev. B* **100**, 184314 (2019).
- [35] B. Höckendorf, A. Alvermann, and H. Fehske, *Phys. Rev. Lett.* **123**, 190403 (2019).
- [36] X. Zhang and J. Gong, *Phys. Rev. B* **101**, 045415 (2020).
- [37] J. Menezes, *Phys. Rev. E* **103**, 052216 (2021).
- [38] J. Knebel, T. Krüger, M. F. Weber, and E. Frey, *Phys. Rev. Lett.* **110**, 168106 (2013).
- [39] A. M. Mambuca, C. Cammarota, and I. Neri, *Phys. Rev. E* **105**, 014305 (2022).